Error-Controlled Iterative Algorithms for Digital Linearization of IMDD-based Optical Fibre Transmission Systems

Jin, Xianqing; Jin, Wei; Zhong, Zhuqiang; Jiang, Shan; Raibhjandari, S.; Hong, Yanhua; Giddings, Roger; Tang, Jianming

Journal of Lightwave Technology

07. May. 2024

Error-Controlled Iterative Algorithms for Digital Linearization of IMDD-Based Optical Fibre Transmission Systems

Xianqing Jin [iD], Wei Jin [iD], Zhuqiang Zhong, Shan Jiang, Sujan Rajbhandari [iD], Yanhua Hong [iD], Roger Philip Giddings [iD], and Jianming Tang [iD]

Abstract—In intensity-modulation and direct-detection (IMDD) single-mode fibre (SMF) transmission systems, the nonlinear operation of square-law detection causes signal-signal beating interference (SSBI) that considerably limits the signal transmission capacity versus reach performance of the systems. To address this challenge, an error-controlled iterative algorithm (ECIA) with extra decision thresholds is proposed to digitally linearize the IMDD transmission systems. In the ECIA, instead of amplitude errors used in previously reported algorithms, the Q^{-2} factor is utilized as an objective function, along with the proposed stochastic gradient descent (SGD) optimization of the thresholds for symbol decision. The thresholds can be adaptively adjusted to reduce decision errors during iterations. To improve the algorithm's adaptivity to various system operation conditions, new constraints are also introduced including maximum step size and/or sign of threshold variation. By making use of the identified optimum key parameters of the ECIA, numerical investigations are conducted of the effectiveness of the proposed scheme in supporting 100 Gb/s 4-level pulse amplitude modulation (PAM4) transmissions over 80 km standard SMFs. Results show that compared with the previously reported decision-directed data-aided iterative algorithm (DD-DIA), the ECIA significantly reduces the power/optical signal-to-noise ratio (OSNR) penalty, required minimum number of iterations (convergence rate) and improves the wavelength drift tolerance. For the ECIA, an OSNR penalty of $\leq$3.8 dB (10% overhead) and a minimum iteration count of 50 are observed for up to 400 km SMF transmissions, showing its robustness to accumulated dispersions of long fibres. More importantly, a pilot-free operation (0% overhead) is also feasible at a cost of a slightly increased OSNR penalty of $\leq$0.5 dB.

Xianqing Jin, Wei Jin, Shan Jiang, Sujan Rajbhandari, Yanhua Hong, Roger Philip Giddings, and Jianming Tang are with the School of Computer Science and Electronic Engineering, Bangor University, LL571UT Bangor, U.K. (e-mail: x.jin@bangor.ac.uk; w.jin@bangor.ac.uk; s.jiang@bangor.ac.uk; s.rajbhandari@bangor.ac.uk; y.hong@bangor.ac.uk; r.p.giddings@bangor.ac.uk; j.tang@bangor.ac.uk).

Zhuqiang Zhong is with the School of Computer Science and Electronic Engineering, Bangor University, LL571UT Bangor, U.K. He is now with the College of Science, Chongqing University of Technology, Chongqing 400054, China (e-mail: zqzhong@cqut.edu.cn).

Index Terms—Chromatic dispersion, digital signal processing, intensity modulation, optical fiber communication, optical signal detection, phase distortion.

I. INTRODUCTION

AS a mainstream for highly cost-sensitive short-reach optical fibre communication systems, intensity modulation and direct detection (IMDD) offers simple system structures with low-cost optoelectronic components [1], [2]. Driven by emerging bandwidth-hungry digital services such as virtual/augmented/mixed reality, IMDD transmission systems are currently confronting unprecedented pressure of upgrading their capacity versus reach performances [3]. A main challenge for upgrading such transmission systems is their inherent nonlinear operation associated with intensity modulation and square-law direct detection. The square-law direct detection operation causes signal-signal beating interference (SSBI) when the phase of an optical signal is distorted by fibre dispersion. In particular, the SSBI effect is much severer for high data rates and/or long lengths of chromatic dispersion (CD)-dominant single-mode fibre (SMF) transmission systems required by converging future optical access networks. To mitigate the SSBI effect, modifications to existing IMDD transmission systems are suggested, including self-homodyne detection with optical polarization demultiplexing of the carrier and the signal [4], generalized/simplified carrier-assisted differential detection [5], Stokes vector reception [6], and the employment of extra and/or costly components including optical phase modulators [7], dual-drive Mach-Zehnder modulators (MZM) [8], [9], delay interferometers [10] and tunable dispersion compensation modules [11]. Such modifications increase the complexity and cost of the transmission systems and their power consumption. To this end, for addressing the SSBI challenge, digital signal processing (DSP)-based techniques are desirable because of their advantages including low complexity and good flexibility as well as no modifications to existing transmission systems. These DSP techniques include, for example, Tomlinson-Harashima precoding [12], [13], Volterra/polynomial nonlinear equalization [14], [15], model-based iteration [16], and combined linear and nonlinear equalization [17]. However, the abovementioned DSP techniques are just capable of partially compensating for the SSBI effect because only the received optical intensity is considered.

It is noted that the CD effect may be partially mitigated by the multi-carrier techniques [18], [19], however the SSBI effect still exists.

To effectively mitigate the SSBI effect, it is necessary to retrieve the received optical phase, which can be used to effectively compensate for fibre dispersion in the digital domain, thus leading to linearized IMDD transmission systems. Based on the Gerchberg-Saxton (G-S) algorithm for the 2D-image construction of X-ray diffraction [20], the phase retrieval of 1D signals was developed for CD pre-compensation [21], [22] or post-compensation [23] for improving signal transmission capacities or reaches of non-return-to-zero on-off keying (NRZ-OOK)-encoded IMDD systems [22], [23] and even quadrature phase shift keying (QPSK)-encoded coherent systems [24]. To further improve the capacity versus reach performances of IMDD transmission systems, a decision-directed data-aided iterative algorithm (DD-DIA) [25] and a multi-constraint iterative algorithm (MCIA) [26] have recently been reported, which support $\geq$100 Gb/s 4-level pulse amplitude modulation (PAM4) IMDD transmission over $\geq$50 km SMFs. Compared with the DD-DIA, the MCIA reduces the required number of iterations and symbol error rate because redundant bits associated with forward error correction (FEC) are reused to reduce decision errors of the PAM symbols in the iterations. However, the DD-DIA and MCIA still require a large number of iterations ($>$100) and a large overhead rate of pilot symbols ($\geq$10%). In addition, in the MCIA the use of FEC in the iterations may cause a large latency. Furthermore, the power and optical signal-to-noise ratio (OSNR) penalties compared with the optical back-to-back (OBTB) systems were not discussed in [25], [26].

To reduce both the total number of iterations and the overhead rate and also to further improve the effectiveness of DSP-based compensation of the SSBI effect, in this paper, we propose an error-controlled iterative algorithm (ECIA) with two extra decision thresholds for error control and new constraints. Compared to the DD-DIA, the power/OSNR penalty is also reduced. As an objective function in the ECIA, instead of the amplitude error in the DD-DIA algorithms, the Q^{-2} factor is applied, along with the proposed stochastic gradient descent (SGD) optimization for adaptive threshold adjustments. To improve the proposed algorithm's adaptivity to various system operation conditions, new constraints on the maximum step size and/or the sign of threshold variation are introduced. As the transmission/convergence performances are dependent on key parameters including learning rates, maximum step size and resolution/clipping-ratio of digital-to-analog/analog-to-digital converters (DACs/ADCs), these parameters are optimized for supporting 100Gb/s PAM4 transmissions over 80 km SMFs. With the optimized parameters, the effectiveness of the proposed ECIA with fixed/adaptive decision thresholds is explored by comparing it with the DD-DIA. Results show that the ECIA significantly reduces the power/OSNR penalty and the required number of iterations by a factor of up to 3 compared with the DD-DIA. In addition, the pilot-free operation (0% overhead) is feasible at a cost of a slightly increased OSNR penalty of $\leq$0.5 dB even for a huge accumulated dispersion of 6400 ps/nm corresponding to 400 km. Furthermore, for practical uncooled lasers with instable wavelengths, the performance tolerance to wavelength drift is investigated, which shows an improved tolerance compared with the DD-DIA.

II. PRINCIPLE OF ECIA

A. ECIA With Extra Two Decision Thresholds

To illustrate the principle of the proposed ECIA, a block diagram of the algorithm in an SMF IMDD system is shown in Fig. 1(a), where the new functions compared to the DD-DIA are highlighted by using a shadow background. At the transmitter, an intensity modulator (IM) is used to convert an analog PAM signal $s(t)$ into an optical signal E_T for propagating over the SMFs. To focus on discussions about the nonlinear operation of the square-law detection in a photodiode (PD) that causes the SSBI effect, the received signal ($r(t)$) can be described in the following form.

$$r\,(t) = \left|\left(\sqrt{s\,(t)}\cdot e^{j\psi(t)}\right)\otimes h\,(t) + w_o\,(t)\right|^2 + w_e\,(t) \quad (1)$$

where $\otimes$ is the convolution operation. $\psi(t)$ is the optical phase at the transmitter mainly due to the modulator's chirp effect. $w_o(t)$ and $w_e(t)$ are the optical and electrical noises, respectively. $h(t)$ is the impulse response of the CD-dominant SMF system, whose (inverse) Fourier transform is denoted as $H(f)$ ($H^{-1}(f)$).

$$H\,(f) = e^{-j\pi DLf^2\lambda^2/c} \quad (2)$$

where D, L, f, λ, and c are the fibre dispersion parameter, distance, analogue frequency, central wavelength, and velocity of light, respectively.

Similar to the conventional iterative algorithms including the DD-DIA [25] and the G-S algorithm, the ECIA requires iterative Fourier transformations (FT) of the channel impulse responses (H) in (2) to mimic the optical signal's forward/backward propagation in the digital domain in order to obtain the accurate phase information. The principle of the DSP process is depicted in Fig. 1(b), where for a measured intensity signal ($\sqrt{r}$) and defined constraints, the CD-induced channel impulse responses are involved back and forth between the image and object domains (received and transmitted signals) during each numerical iteration process. An error control is introduced to reduce both the symbol decision errors in the object domain and required minimum number of iterations to converge bit error rates (BERs).

To apply DSP-based linearization algorithms for the effective compensation of the CD at the receiver, the received signal is digitized by an ADC followed by synchronization and serial-to-parallel (S/P) conversion (required for FT). The procedure of the ECIA is described below, which contains the following 5 steps:

1. The square-root of the digitized signals (parallel samples) combined with an estimated optical phase is used to reconstruct the received optical signal $\sqrt{r}e^{-j\angle\hat{E}_R}$. The initial phase ($\angle\hat{E}_R$) is set to linearly increase from 0 to 2π across the parallel samples.
2. After the CD compensation (multiplying by H^{-1}) in the frequency domain, a matched filter (MF) and a downsampling (DS) process are applied.
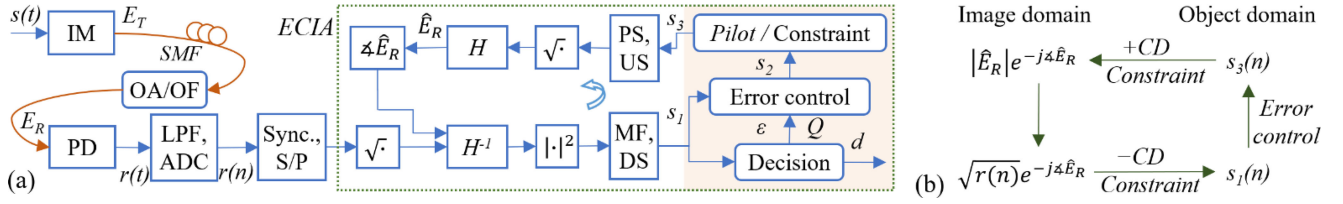
Fig. 1.   (a) Block diagram of an SMF IMDD system with ECIA and (b) the principle of ECIA. US/DS: up/down-sampling. Sync.: synchronization.

3. The symbol decision with a normalized threshold of 0.5 is applied to signal s_1. Once the decision errors are converged or the iteration index reaches their defined maximum values, the final decided symbols are obtained. Otherwise, the error control process is applied to adaptively adjust the decision errors in each iteration procedure.

4. As pseudorandom pilot symbols are digitally prearranged at a symbol interval at the transmitter using a conventional approach, the pilot symbols and the decided symbols are selectively chosen according to the defined constraints in reconstructing the transmitted symbol sequence s_3.

5. Following the upsampling (US), pulse shaping (PS), square-root operation and insertion of CD-induced phase, the received optical signal ($\hat{E}_R$) is reconstructed. The phase of $\hat{E}_R$ is extracted to update the input signal $\sqrt{r}e^{-j\angle\hat{E}_R}$ for use in the next iteration starting from step 1.

In the previously reported iterative algorithms [25], [26], an objective function, ζ^2, is set to be the amplitude error or mean square error (MSE) between the reconstructed optical signal ($\hat{E}_R$) and the actually measured intensity ($\sqrt{r}$).

$$\zeta^2 = E\left[\left(\left|\|\hat{E}_R\| - \sqrt{r}\right|/E\left[\sqrt{r}\right]\right)^2\right] \quad (3)$$

where E denotes the expectation operation. For the DD-DIA, the decided symbols (d) with a normalized threshold of 0.5 are randomly selected with a Bernoulli distribution in an iteration to minimize the ζ^2 value [25]. Because of many possible solutions of $\hat{E}_R$ corresponding to a minimum of ζ^2, the estimated optical phase may not reflect its real value. To address this challenge, we propose an objective function of the Q^{-2} factor calculated from the decision errors.

$$Q^{-2} = \frac{1}{K-1} \sum_{k=0}^{K-2} \left[\frac{(\sigma_{k+1} + \sigma_k)}{(\mu_{k+1} - \mu_k)}\right]^2 \quad (4)$$

where μ_k and σ_k are the mean and standard deviations of the estimated signal s_1 corresponding to the decided symbol d_k. K is the number of PAM levels. As a uniform distribution of the PAM levels is assumed in this paper, $\mu_{k+1} - \mu_k$ is equal to the distance between two adjacent PAM levels, Δ. It is easy to understand that the PAM signal's ideal levels ($d_{0,1,..,K-1}$) can be estimated by the signal's mean or channel estimation.

Compared with ζ^2 related to the optical intensity only, Q^{-2} is directly determined by the estimated real-valued transmitted signals. Therefore, in theory, a unique solution of $\hat{E}_R$ exists for a minimum Q^{-2}. To effectively minimize Q^{-2}, the proposed
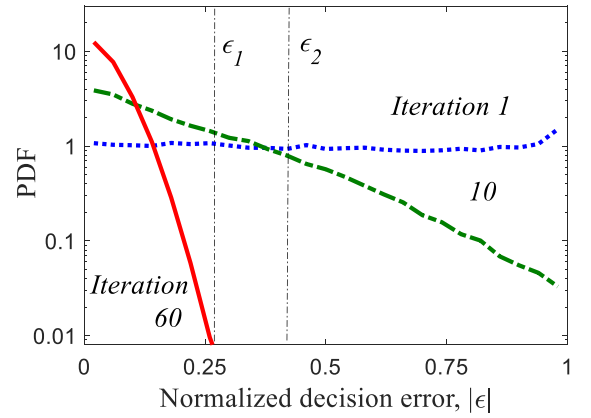

Fig. 2.   Normalized decision error distributions varied with iteration index.

ECIA introduces an error control to the decision errors ($\varepsilon = (s_1 - d)/\Delta$) with extra two thresholds (ε_1, ε_2) expressed below:

$$s_2 = \begin{cases} s_1 - \varepsilon \cdot \Delta, & |\varepsilon| < \varepsilon_1 \\ s_1 - (\varepsilon - \varepsilon/|\varepsilon|) \cdot \Delta, & |\varepsilon| > \varepsilon_2 \\ s_1, & \varepsilon_1 \leq |\varepsilon| \leq \varepsilon_2 \end{cases} \quad (5)$$

The idea of the ECIA is originally from the fact that the decision errors normally occur around decided symbol values (d) so that the initial errors with a uniform distribution are expected to slowly converge toward zero during iterations as shown in Fig. 2. For $|\varepsilon| < \varepsilon_1$, the symbols have a high probability of being decided correctly in a normal way. For $|\varepsilon| > \varepsilon_2$, an extra error control of $(\varepsilon - \varepsilon/|\varepsilon|) \cdot \Delta$ is applied to the symbols that may be wrongly decided in the normal way. For symbols with $\varepsilon_1 \leq |\varepsilon| \leq \varepsilon_2$, no symbol decision is made because of a possibly equal probability of correct or wrong decisions. The error control is conducted when the BER or Q^{-2} is below a specific value (a BER of 0.03 in this paper) during the iterations, above which s_2 is assumed to be equal to s_1.

Following the error control, the prearranged pilot symbols are used to periodically update the received/calculated pilot symbols in the signal sequence (s_2) at an iteration interval [25]. The overhead rate of the pilot symbols, δ, is equal to the inverse of the pilot symbol interval. For example, a symbol interval of 10 corresponds to an overhead rate of 10%. In addition, an extra constraint can also be applied by clipping the amplitude of s_2 beyond the target range ($d_0 \sim d_{K-1}$) below:

$$s_2 \in [d_0, d_{K-1}] \quad (6)$$

B. Stochastic Gradient Descent (SGD)-based Optimization of (adaptive) Threshold ε_2

The optimum values of the extra decision thresholds (ε_1, ε_2) in (5) depend on various factors including signal to noise ratio (SNR) and fibre dispersion/lengths. The thresholds can be fixed at specific values or adaptively adjusted according to the objective function of Q^{-2}. In general, the ε_1 value determines possibly correct decisions of a majority of symbols after several initial iterations, whilst the ε_2 value mainly affects possibly wrong decisions of symbols. Therefore, our target is to optimize ε_2 when ε_1 is fixed at a specific value. Given the iterative feature of the ECIA, the SGD-based optimization is proposed for adaptively updating the threshold, ε_2'.

$$\varepsilon_2' = \varepsilon_2 - \eta \cdot \nabla Q^{-2}(\varepsilon_2) \qquad (7)$$

where η is the learning rate, ∇ is a gradient operator. Owing to the optical/electrical noises, the estimated $Q^{-2}(\varepsilon_2)$ varies with iteration. To mitigate the noise effect, the new threshold, ε_2', is updated every M_Q iterations with an average of $Q^{-2}(\varepsilon_2)$ in the M_Q iterations. In addition, as symbols may be wrongly decided with the variable threshold, the objective function may fluctuate in different iterations. To improve the robustness of the ECIA, the prearranged pilot symbols are applied in (4) for the accurate calculation of the objective function, $Q_p^{-2}(\varepsilon_2)$. (7) is applied when $\nabla Q^{-2}(\varepsilon_2)$ and $\nabla Q_p^{-2}(\varepsilon_2)$ have the same sign. Although the accuracy of $Q_p^{-2}(\varepsilon_2)$ is high, $Q^{-2}(\varepsilon_2)$ instead of $Q_p^{-2}(\varepsilon_2)$ must be applied in (7) to indicate decision errors of the information symbols instead of pilot symbols. These constraints can be described as follows.

$$\nabla Q^{-2}(\varepsilon_2) \cdot \nabla Q_p^{-2}(\varepsilon_2) > 0 \qquad (8)$$

$$\left| \eta \cdot \nabla Q^{-2}(\varepsilon_2) \right| \le \varepsilon_s \qquad (9)$$

where ε_s is the maximum step size that limits the maximum variation of ε_2 in an iteration. If constraint (8) is not satisfied, a small variation of ε_2 is added to ensure an update of $\varepsilon_2' = \varepsilon_2 - 2.5 \times 10^{-3} \cdot sgn(\nabla Q_p^{-2}(\varepsilon_2))$. $sgn()$ is the sign function of a number. If constraint (9) is not satisfied, (7) can be modified as $\varepsilon_2' = \varepsilon_2 - \varepsilon_s \cdot sgn(\nabla Q^{-2}(\varepsilon_2))$. The estimated ε_2' is controlled in a range of [0.05, 0.45]. The initial threshold ε_2 is set to be 0.4 when the iteration index is smaller than 25.

For a pilot-free operation, constraint (8) is not applicable, as such a local solution of ε_2 may occur causing calculated ε_2' values remaining relatively low for many iterations when the BER converges at a relatively high value. To avoid the occurrence of the local solution, a new threshold ε_2' is set to be the upper limit of 0.45 if the values of five successively updated ε_2' with a standard deviation of <0.025 remain lower than 0.4.

As an example, Fig. 3 shows the threshold ε_2 adaptively adjusted to minimize Q^{-2} corresponding to BER in an 80 km SMF transmission system. In the figure, the default parameters in Table I are applied. SGD optimization is applied after 20 iterations such that the Q^{-2} calculated with decided symbols significantly decreases to the levels of Q_p^{-2} calculated with pilot symbols. After 25 iterations, the threshold decreases from 0.4 to 0.18, which results in a small fluctuation of Q^{-2} and BER around the iteration of 40. Such a fluctuation does not degrade
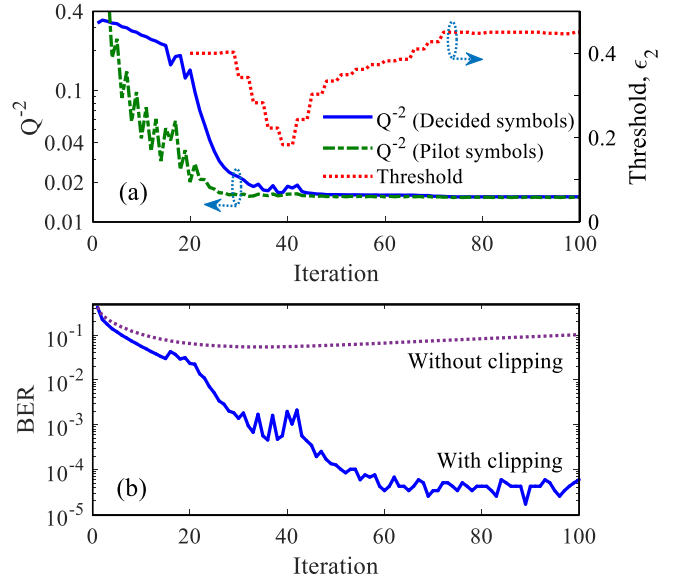
Fig. 3.   Example of adaptive threshold (ε_2) and BER/ Q^{-2} optimized by SGD.

TABLE I
DEFAULT PARAMETERS

Parameters	Default setting	Parameters	Default setting
Modulation format	PAM4	Threshold, ε_1	0.25
Raw bit rate	100 Gb/s	Initial threshold, ε_2	0.4
Roll-off factor (PS), α	0.1	Learning rate, η	4
Intensity modulator	MZM	Maximum step, ε_s	0.06
Modulation index	0.6	M_Q	3
Launch power	-2 dBm	Pilot symbol interval	10
Fibre length	80 km	Iteration interval	2
Dispersion parameter, D	16 ps/nm/km	Resolution (DACs, ADCs)	7, 8 bits
Thermal noise (PIN)	10×10^{-12} A/Hz$^{1/2}$	Clipping ratio (DACs, ADCs)	10, 14 dB
Quantum efficiency	0.8	Bandwidth (OF)	82.5 GHz
Wavelength	1550 nm	Bandwidth (LPF)	41.3 GHz

the final BER performance but contributes to a further decease in BER when the threshold increases to 0.45. This can also be explained by introducing a disturbance in Q^{-2} or BER to avoid a local solution of ε_2 corresponding to a relatively high BER in the ECIA with the SGD optimization. After 60 iterations, the BER converges towards a relatively low value. It is noted that before the BER converges at a low value the curves of Q^{-2} are higher but less fluctuated than Q_p^{-2}, confirming the right choice of Q^{-2} in (7). In addition, the BER obtained with clipping in constraint (6) is significantly reduced compared with no clipping constraint.

III. OPTIMIZATION OF KEY PARAMETERS

Based on the principle of the ECIA, key parameters affecting the algorithm's convergence/transmission performance need to be numerically optimized for maximizing its transmission/convergence performances. The numerical optimizations

are undertaken under the following conditions: at the transmitter, 100 Gb/s PAM4 analog electrical signals are generated from a pseudorandom sequence (length: 1.3×10^5 bits) with square-root raised cosine (SRRC) filter-based pulse shaping and DACs. An MZM with a frequency chirp-free operation at a wavelength of 1550 nm and a modulation index of 0.6 is used as an IM to convert the electrical signals into an optical signal. The optical launch power is fixed at -2 dBm. The optical signal propagation over 80 km standard SMFs is simulated by a split-step Fourier method (step length: 0.5 km). The received optical signal is amplified by an optical amplifier (OA) followed by an optical filter (OF) before the direct detection in a PIN photodiode. Optical noise is loaded on the received optical signal according to the OSNR defined within a spectral resolution of 0.1 nm, which is fixed at 36 dB. The detected electrical signal passes an ideal low pass filter (LPF) with a bandwidth of 41.3 GHz and an ADC operating at a sampling rate of twice the signal baudrate. It is assumed that the nonlinearity of the MZM can be pre-compensated at the transmitter, and the received samples are ideally synchronized at the receiver. In practice, the synchronization process can be carried out with a preamble in the front of the signal sequence. The fast Fourier transform (FFT) is applied to the input parallel sample signal for CD compensation in the frequency domain. For theoretical/numerical evaluations, the number of parallel samples is set to be equal to the number of generated samples at a sampling rate of twice of the signal baudrate. The maximum number of iterations is 200. All the default parameters mentioned above are summarized in Table I.

A. Decision Threshold (ε_1)

The first key parameter is decision threshold ε_1 that affects the number of symbols with possibly correct decisions in the iterations. In Fig. 4(a), the curves of BER versus decision threshold ε_1 are compared for different received optical powers (ROPs). An optimum value of $\varepsilon_1 = 0.25$ is observed for achieving the lowest BERs regardless of the ROP values. For a small threshold of $\varepsilon_1 < 0.25$, the portion of decided symbols with errors in the range $|\varepsilon| < \varepsilon_1$ is relatively small, which limits the role of symbol decision in the error control. As a result, the BER decreases with increasing ε_1. For $\varepsilon_1 \geq 0.3$, the number of symbols with wrong decisions is high compared with relatively small ε_1 values. This causes a slight increase in BER. Thanks to the error control with adaptive threshold ε_2 after applying ε_1, the BERs for $\varepsilon_1 \geq 0.3$ remain relatively low but still higher than their lowest values. For the largest ε_1 of 0.45 in the figure, the effect of decision threshold ε_1 can be ignored. In such a case, the application of only adaptive threshold ε_2 cannot further improve the BER performance. This suggests the necessity of decision threshold ε_1 in the ECIA with SGD. To simplify the DSP algorithm and improve its effectiveness, ε_1 is fixed at 0.25, whilst ε_2 is adaptively adjusted in different operation conditions.

B. Learning Rate (η) and Maximum Step Size (ε_s)

The learning rate (η) and maximum step size (ε_s) play an important role in determining the convergence and transmission performances of the algorithm. A large η or ε_s benefits fast
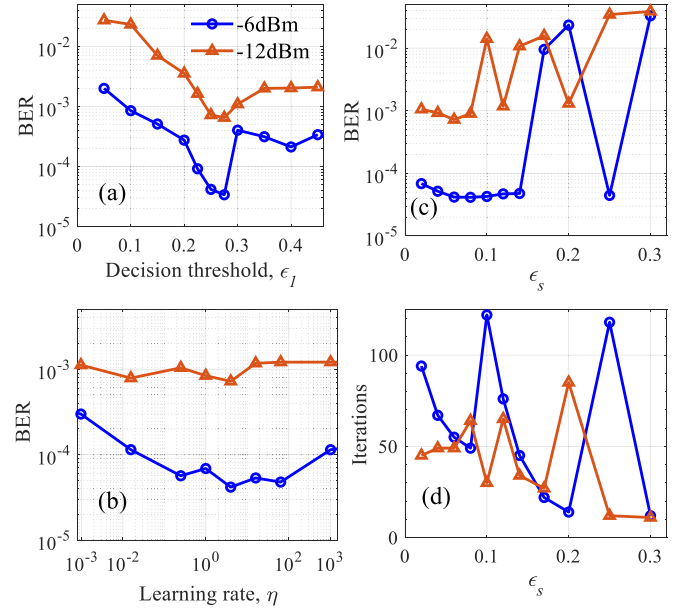

Fig. 4. Impacts of decision threshold ε_1 (a), learning rate η (b) and maximum step size ε_s (c-d) on BER or required number of iterations. ROP: -6 dBm (blue), -12 dBm (red).

convergence but may lose stability for cases where BERs are low, thus optimum values of η and ε_s are desired to balance fast convergence and low BER. To achieve such an optimum balance, the learning rate (η) is firstly optimized in Fig. 4(b) where ε_s is equal to 0.06. For a high ROP (-6 dBm), the BER varies significantly with the learning rate, whilst for a small ROP (-12 dBm), the BER remains at $\sim 10^{-3}$. This indicates the advantage of the SGD for the high received optical power (or relatively low noise) condition. In Fig. 4(b), the minimum BER of 4×10^{-5} for a ROP of -6 dBm is shown at $\eta = 4$, which is used to investigate the impact of ε_s in Fig. 4(c)–(d). For the ROP of -12 dBm (-6 dBm), the BER remains at $\sim 1 \times 10^{-3}$ ($\sim 4 \times 10^{-5}$) in the range $0.02 < \varepsilon_s < 0.08$, above which a large variation in BER or the required number of iterations are observed. The variation may be because a relatively large ε_s (≥ 0.08) with poor stability increases the risk of significantly increased number of wrongly decided symbols, thus the BER is degraded. As the defined maximum number of iterations is 200, the high BER values of $> 10^{-2}$ may be estimated before the BER is converged. On the other hand, for a relatively small ε_s (< 0.06), the BER is low but requires an increased number of iterations for a ROP of -6 dBm as shown in Fig. 4(d). Therefore, the optimum value of ε_s is 0.06.

C. Resolution and Clipping Ratio of DACs/ADCs

As received signal amplitudes distorted by fibre dispersion and SSBI vary randomly, a high-resolution DAC/ADC with a large clipping ratio (input/output range) is normally required for reducing quantization noise and clipping distortion. From a practical system design point of view, for relaxing the hardware requirement for the optical phase retrieval, it is necessary to study the minimum (bit) resolution and clipping ratio. The
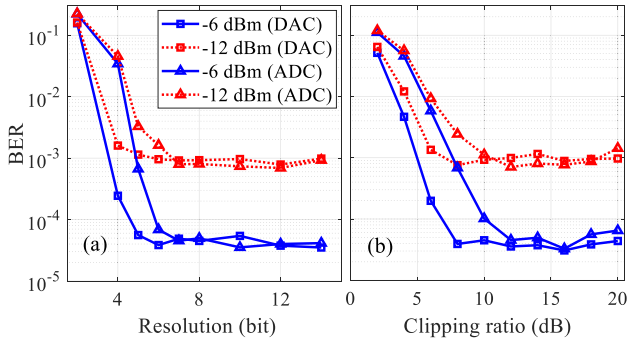
Fig. 5. Impacts of resolution/clipping-ratio (DAC/ADC). ROP: -6 dBm (blue), -12 dBm (red). DAC/ADC: square/triangular markers.

impacts of the resolution and clipping ratio on BER are presented in Fig. 5. The BER significantly decreases with increasing resolution and clipping ratio of the DAC/ADC from 2 to 6 bits and from 2 to 12 dB, respectively. For the ROPs of -6 and -12 dBm, error floors occur at a resolution of ≥ 7 (8) bits and a clipping ratio of ≥ 10 (14) dB for the DAC (ADC). An extra 1 bit of resolution is required for ADC due to the 4 dB increment in clipping ratio shown in the figure. For a hard-decision FEC limit of 3.8×10^{-3}, relatively low resolutions (clipping ratio) of 4 bits and 6 bits (6 dB and 8 dB) may be required for the DAC (ADC). To explore the best BER performance of the ECIA, in following simulations, the resolutions (clipping ratio) of the DAC and ADC are set to be 7 bits and 8 bits (10 dB and 14 dB), respectively. It is noted that for very short SMF transmission or OBTB cases, the DAC/DAC requirement can be relaxed further, which is however not the focus of the present work.

IV. TRANSMISSION AND CONVERGENCE PERFORMANCES

With the optimized parameters in Section III, the proposed ECIA is verified in this section, where the DD-DIA is also applied for performance comparisons [25]. The two ECIA schemes with and without SGD correspond to adaptive and fixed values of ε_2. As the DD-DIA requires a relatively large number of iterations for obtaining a converged BER performance, the maximum number of iterations for the DD-DIA is set to be 320.

A. Evaluation of Objective Functions

To evaluate the validity of the objective functions in (3)–(4), convergence performances in amplitude/phase errors and BER/Q^{-2} are compared for 100 Gb/s over 80 km SMF IMDD systems in Figs.6(a-c). As shown in the figures, the two ECIA schemes with and without SGD have similar performances, and their BER values converge much faster than the DD-DIA. Only approximately 30 and 50 iterations are required for approaching the FEC limit and converged BERs, respectively. Prior to achieving the converged BER at iteration 50, the amplitude error for the ECIA with SGD fluctuates more rapidly than the other schemes because of the adaptively varied threshold shown in Fig. 6(d). However, its phase error and Q^{-2} decrease with less fluctuation as the iteration count increases. The differences in amplitude error, phase error and Q^{-2} at iteration 200 between the ECIA and

DD-DIA are approximately 3%, 16% and 36% of their average values, respectively. As a result, the schemes (ECIA) with an objective function of Q^{-2} have relatively low BERs. Although the converged amplitude errors for all the cases considered here are almost equal, the ECIA with an adaptive threshold (ε_2) offers the lowest BER and phase errors because of its adaptivity to various levels of noise/error. This indicates that the amplitude error in (3) does not reflect the reconstructed optical signal at a high accuracy. The objective function in (4) can thus be used to improve the convergence and BER performances, along with the decision error control.

Given the fact that an accurate decision threshold significantly affects the BER performance of the ECIA, it is necessary to investigate the impact of fixed values of ε_2 on BER and the required number of iterations as shown in Fig. 6(e)–(f). To achieve the lowest BERs for the ECIA with no SGD (fixed thresholds), optimum thresholds of 0.325 and 0.275 are identified for the ROPs of -12 dBm and -6 dBm, respectively. Compared with the optimum ε_1 values of 0.25 identified in Fig. 4(a), the optimum values of fixed ε_2 are dependent on ROP or link noise level. The reason is that a low ROP causes a large variance of decision errors that normally requires a large threshold (ε_2). It is interesting to note that the lowest BER ($\sim 10^{-3}$) at the optimum fixed threshold of 0.325 is slightly larger than the BER with SGD-based adaptive thresholds. However, its required number of iterations (~ 65) at $\varepsilon_2 = 0.325$ is higher than the SGD case (~ 50) although the required number of iterations at $\varepsilon_2 \geq 0.35$ is less than 50. This indicates that a fixed threshold (ε_2) may offer similar BER performance as the adaptive threshold with SGD but possibly requires a large iteration count. In addition, the optimum value of the fixed threshold (ε_2) depends on SNR, fibre dispersion and iteration index from which the ε_2 is applied. This imposes challenges in estimating channel conditions for practical systems. On the other hand, the SGD is applied to automatically search optimum values of ε_2, this offers technically good adaptivity against various operation conditions. In following discussions, the ECIA with SGD is considered to represent the ECIA scheme by default.

B. Comparisons Between (pilot-free) ECIA and DD-DIA

For both the ECIA and the DD-DIA, pseudorandom pilot symbols prearranged at the transmitter are used to replace the received/estimated pilot symbols at a defined iteration/symbol interval at the receiver [25]. To explore the effectiveness of the pilot symbols, the transmission performances are compared between the ECIA and the DD-DIA in Fig. 7. In general, the ECIA outperforms the DD-DIA in terms of BER and required number of iterations for different iteration/symbol intervals. In Fig. 7(a)–(b), for the ECIA the curves on iteration interval are much flatter than the DD-DIA, indicating its less dependence on iteration interval. For the ROPs of -6 dBm or -12 dBm, the difference in BER between the ECIA and DD-DIA increases with increasing the symbol/iteration interval until the BER reaches a relatively high value. The main reason for the observed difference is that in the DD-DIA the decided symbols are randomly selected without considering the error features and the
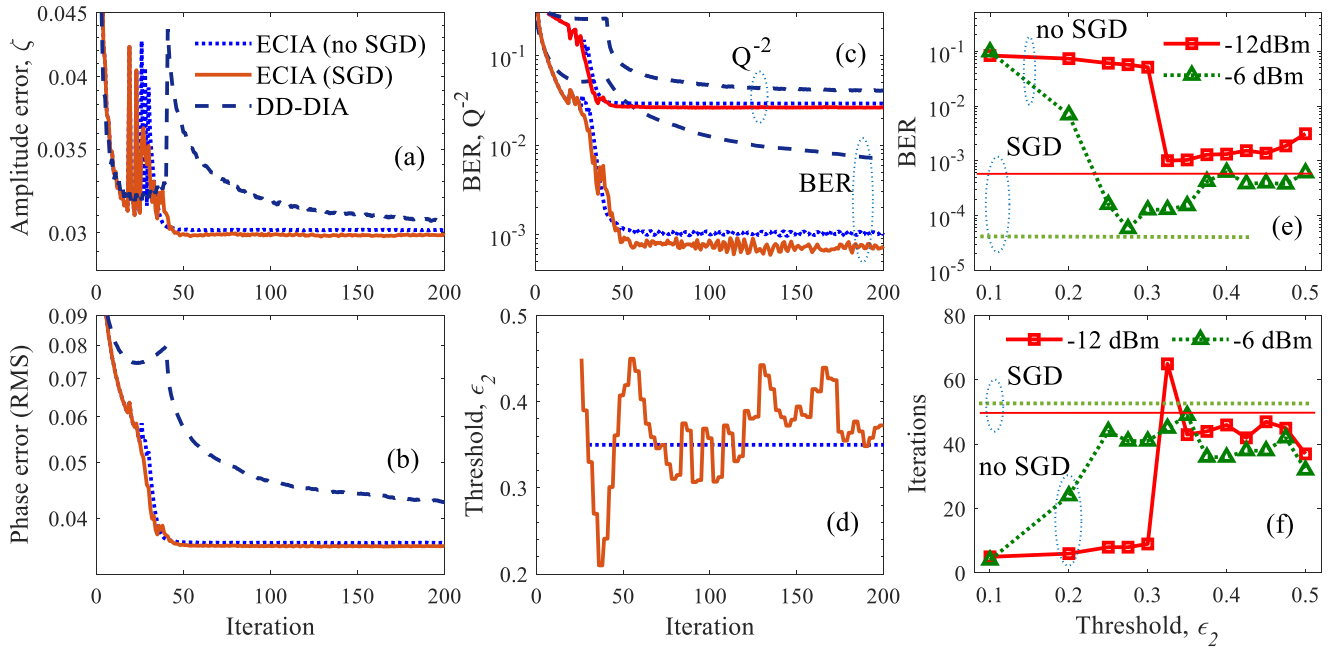
Fig. 6.   (a)–(d) Comparisons in amplitude/phase errors, BER, Q^{-2}, threshold (ε_2) between the ECIA without/with SGD (dotted/solid lines), and the DD-DIA (dashed curves), and (e-f) BER and required number of iterations at different fixed values of ε_2 for ROPs of -12 dBm (red) and -6 dBm (green).
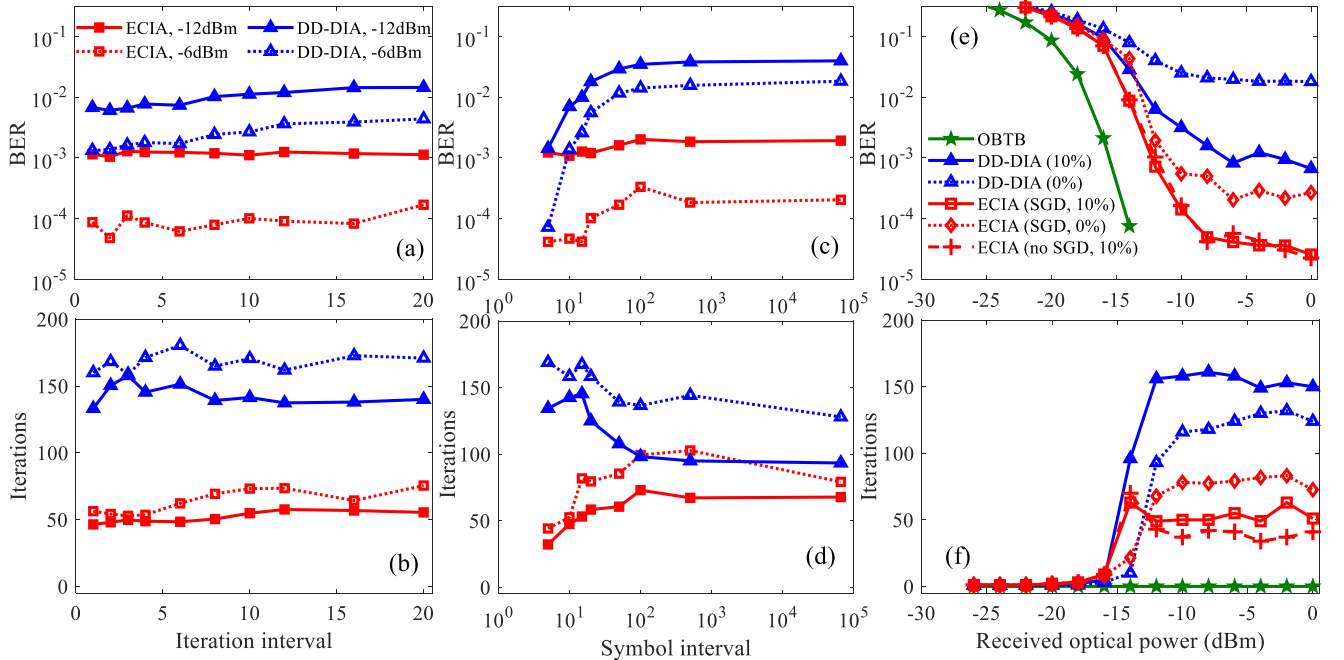

Fig. 7.   Comparison in BER and required number of iterations affected by the (a)–(b) (pilot) iteration interval, (c)–(d) (pilot) symbol interval and (e)–(f) ROP. (a)–(d): red/blue curves for ECIA/DD-DIA, solid/dotted curves for ROPs of -12 dBm /-6 dBm. (e)–(f): solid/dotted curves for overheads of 10%/0%.

pilot symbols are mainly used for reducing the errors of decided symbols. As a result, the BER with the DD-DIA significantly degrades with increasing the symbol interval in Fig. 7(c). The ECIA, by contrast, introduces selective symbols decided with fixed and adaptive thresholds in SGD so that the pilot symbols are less important for reducing the BER. Therefore, for the ECIA the BER and required number of iterations remains relatively

low even when the symbol interval increases from 5 to the whole symbol length of 65536, this means that the ECIA can be treated as a pilot-free operation. As shown in Fig. 7(a)–(d), compared to the DD-DIA, the BER/convergence performances of the ECIA are less dependent on the number or occurrence frequency of pilot symbols. The pilot-free operation may be possible at a small cost of power/OSNR as discussed below.
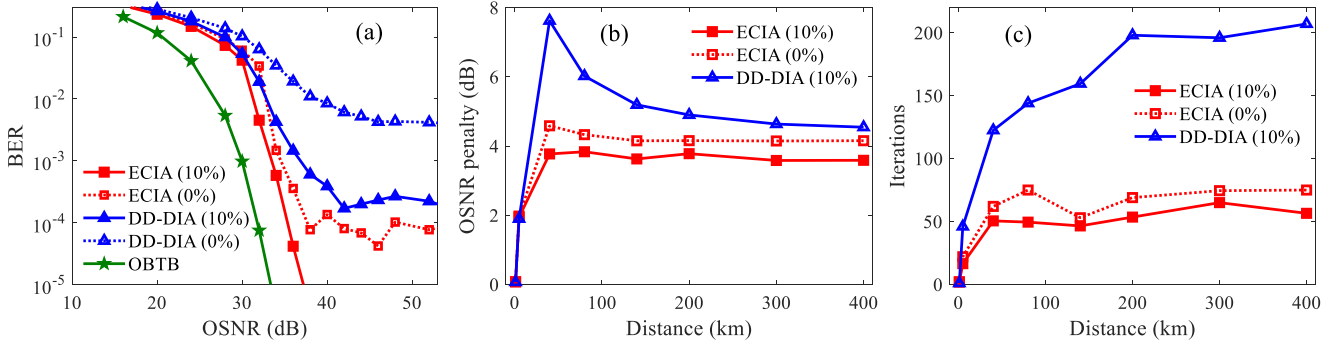
Fig. 8. (a) BER as a function of OSNR over 80 km SMFs, (b) OSNR penalty and (c) corresponding number of iterations at different distances. ECIA/DD-DIA: red-square/blue-triangle markers. Overheads of 10%/0%: solid/dotted curves.

C. Power/OSNR Penalty

To further demonstrate advances of the ECIA with the SGD and/or pilot-free operation (δ: 0%), the BER and required number of iterations at different ROPs are presented in Fig. 7(e)–(f). Compared with the OBTB case, a power penalty of 3.2 dB (4.1 dB) at the FEC limit is observed for the 80 km SMF link based on the ECIA with the SGD and a 10% (0%) overhead. Such a power penalty is much less than the DD-DIA (6.4 dB). The pilot-free operation can be realized with the ECIA at a cost of an extra power penalty of 0.9 dB. The DD-DIA with the pilot-free operation cannot provide BER less than the FEC limit. The curves for the two ECIA schemes with 10% overheads almost overlap, confirming the validity of the SGD in the ECIA. It is noted that the error floor with the ECIA with a 10% overhead is over one order of magnitude lower than the DD-DIA. This is due to the improved accuracy of the reconstructed optical signal with the ECIA. For achieving BERs less than the FEC limit, the required minimum number of iterations for the ECIA and DD-DIA are approximately 50 and 155, respectively. Therefore, the power penalty and convergence rate with the ECIA are improved by a factor of 2 and 3 respectively.

Apart from the abovementioned power penalty, Fig. 8(a) shows the OSNR dependent BER performance where the ROP is taken to be a relatively large value (-6 dBm). The trends of the BER versus OSNR curves are similar to those in Fig. 7(e). The OSNR penalty for the ECIA with 10% and 0% overheads and the DD-DIA are 3.8, 4.3, and 6.0 dB, respectively. Even for large OSNRs, the DD-DIA (δ: 0%) still cannot reach the FEC limit. For the ECIA (δ: 10%), its BER of less than 10^{-5} is shown at OSNRs of > 38 dB in Fig. 8(a). By comparing Figs. 8(a) and 7(e), it is clear that the error floor shown in Fig. 7(e) is due to the OSNR limitation. For the ECIA with a 0% overhead, owing to the increased OSNR at a relatively high ROP, the BER corresponding to the error floor is about 10^{-4}, which is, however, still lower than the DD-DIA.

The impact of transmission distance (fibre dispersion) on OSNR penalty is explored in Fig. 8(b)–(c), where the OSNR penalty and corresponding minimum number of iterations are plotted as a function of transmission distance up to 400 km. Such a long distance is used to demonstrate the effectiveness of the proposed technique in compensating large fibre dispersion.
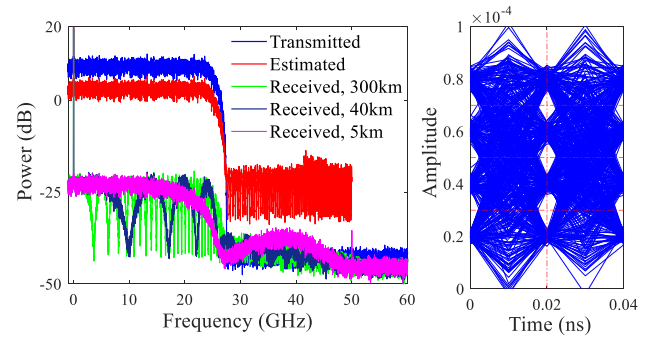

Fig. 9. Power spectra of transmitted/received/estimated electrical signals and an eye diagram at a BER of 3×10^{-3} (300 km, ECIA with a 10% overhead).

For short distances of several kilometers, as the fibre dispersion is small, the penalty curves are nearly overlapped indicating similar performances. For distances of $\geq$40 km (640 ps/nm), the OSNR penalty for the ECIA (δ: 10%) remains at approximately 3.8 dB, which is $\leq$0.5 dB and $\geq$0.7 dB lower than the ECIA (δ: 0%) and the DD-DIA (δ: 10%). Meanwhile, the required minimum number of iterations for the ECIA (δ: 0% and 10%) is approximately 50~60, which is at least 2.5 times smaller than the DD-DIA. On the other hand, for relatively long distances, the required minimum number of iterations for the DD-DIA increases from 123 (40 km) to 207 (400 km). The main reason for the increased (almost constant) penalty over $\leq$40 km ($\geq$80 km) SMFs is the frequency selective power fading effect, which causes power loss of the received signals. For $\leq$ 40 km ($\geq$80 km) SMFs with a small (large) number of dips in the received signal spectral regions as shown in Fig. 9, the signal power loss increases (almost remains constant) with increasing distance. The penalty peak for the DD-DIA with a fixed threshold of 0.5 may be because the algorithm has relatively limited adaptivity and robustness to different transmission distances, thus resulting in varied distortions in signal amplitude and phase. Although the spectra of the received electrical signals after long-distance transmissions (300km, 4800 ps/nm) are seriously distorted, the ECIA can still be used to recover the received signal spectra, as illustrated in Fig. 9. The estimated and transmitted signal spectra are similar over the signal spectral range, beyond which residual
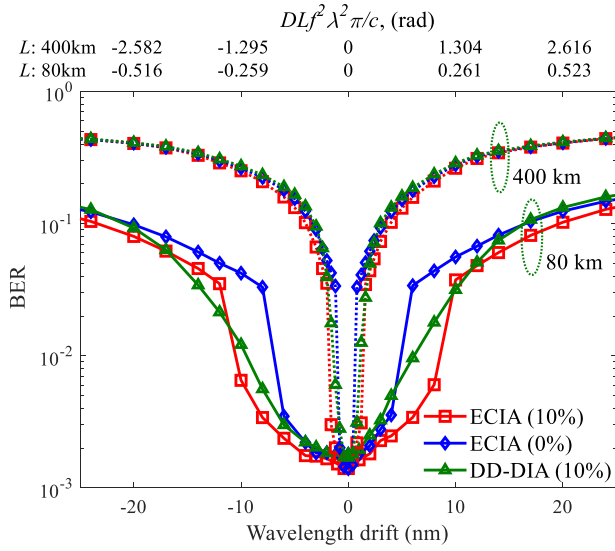
Fig. 10. BER versus wavelength drift or phase error ($DLf^2\lambda^2\pi/c$) at distances of 80 km and 400 km. f: 25 GHz.

frequency components can be digitally filtered out. As a result, a clear eye diagram at a BER of 3×10^{-3} after 300 km SMF transmissions is also presented in the same figure.

D. Tolerance Against Wavelength Drift

In practical conditions where uncooled lasers are preferred, the wavelength of the lasers/IMs may vary with time/temperature due to variations in effective refractive index of the laser materials. Such wavelength drift degrades the CD-induced phase distortions, which are proportional to the square of wavelength, as shown in (2). To investigate the tolerance of the proposed ECIA against wavelength drift, a fixed wavelength error (drift) is added in (2) for the CD compensation at the receiver. The BER performances over 80 km (1280 ps/nm) and 400 km (6400 ps/nm) SMF transmissions are illustrated in Fig. 10. For fair comparisons, the OSNR is adjusted to ensure a BER of around 1.5×10^{-3} at an ROP of -6 dBm when the wavelength drift is zero. Such an OSNR is used for non-zero wavelength drift cases. As seen in Fig. 10, both the ECIA and DD-DIA are sensitive to wavelength drift especially for long-distance transmissions (400 km). A wavelength drift tolerance of up to ±7.2 nm (±1.5 nm) after 80 km (400 km) SMF transmissions corresponding to a phase error of ±0.19 rad (frequency: 25 GHz) by the ECIA (10% overhead) is obtainable, over which the corresponding BERs are less than the FEC limit. Compared with the DD-DIA, the ECIA with a 10% overhead improves the wavelength drift tolerance by approximately 2.4 nm over 80 km SMFs, which is approximately 5 times 0.5 nm over 400 km SMFs. This is because the ECIA contributes to an improved power/OSNR penalty and BER, and the phase variation in (2) can be considered to linearly increase with wavelength drift when the ratio between the wavelength drift and the wavelength is relatively small ($<1\%$ in Fig. 10). For very long transmission distances of over 400 km, an accurate estimation/measurement

of the wavelength may be required. However, such a requirement may not be necessary for relatively short distances of up to 80 km.

V. CONCLUSION

To address the challenge of the nonlinear operation of square-law detection, an error-controlled iterative algorithm with extra decision thresholds has been proposed to digitally linearize the IMDD-based SMF transmission systems. Based on the principle of the ECIA, an objective function of the Q^{-2} factor instead of the amplitude error used in previously reported algorithms is utilized along with the proposed SGD-based optimization of adaptive decision thresholds. To improve the algorithm's adaptivity to various system operation conditions, new constraints are introduced including maximum step size and/or sign of threshold variation. With the identified optimum key parameters of the ECIA, the effectiveness of the proposed scheme has been numerically explored in 100 Gb/s PAM4 IMDD transmissions over 80 km standard SMFs. Results have shown that compared with the previously reported DD-DIA the ECIA significantly reduces the power/OSNR penalty, required minimum number of iterations (convergence rate) and improves the wavelength drift tolerance by a factor of up to 3. For the ECIA, an OSNR penalty of ≤3.8 dB (10% overhead) and a minimum iteration count of 50 are observed for up to 400 km (6400 ps/nm) SMF transmissions, showing its robustness to accumulated dispersions of long fibres. More importantly, the pilot-free operation (0% overhead) is also feasible at a cost of a slightly increased OSNR penalty of ≤0.5 dB. Therefore, the proposed ECIA has great potential for future high capacity and/or long reach IMDD transmission systems.

REFERENCES

[1] W. Heni et al., "Ultra-high-speed 2:1 digital selector and plasmonic modulator IM/DD transmitter operating at 222 GBaud for intra-datacenter applications," *J. Lightw. Technol.,* vol. 38, no. 9, pp. 2734–2739, May 2020.

[2] T. Wettlin, S. Calabrò, T. Rahman, J. Wei, N. Stojanovic, and S. Pachnicke, "DSP for high-speed short-reach IM/DD systems using PAM," *IEEE J. Lightw. Technol.,* vol. 38, no. 24, pp. 6771–6778, Dec. 2020.

[3] J. S. Wey, "The outlook for PON standardization: A tutorial," *J. Lightw. Technol.,* vol. 38, no. 1, pp. 31–42, Jan. 2020.

[4] Y. J. Wen, A. Li, Q. Guo, Y. Cui, and Y. Bai, "200G self-homodyne detection with 64QAM by endless optical polarization demultiplexing," *Opt. Exp.,* vol. 28, no. 15, pp. 21940–21955, Jul. 2020.

[5] H. Ji et al., "Carrier assisted differential detection with generalized and simplified receiver structure," *IEEE J. Lightw. Technol.,* vol. 39, no. 22, pp. 7159–7167, Nov. 2021.

[6] D. Che, C. Sun, and W. Shieh, "Maximizing the spectral efficiency of Stokes vector receiver with optical field recovery," *Opt. Exp.,* vol. 26, no. 22, pp. 28976–28981, Oct. 2018.

[7] S. Ishimura, H.-Y. Kao, K. Tanaka, K. Nishimura, and M. Suzuki, "SSBI-free direct-detection system employing phase modulation for analog optical links," *J. Lightw. Technol.,* vol. 38, no. 9, pp. 2719–2725, May 2020.

[8] W. Wang, F. Li, Z. Li, Q. Sui, and Z. Li, "Dual-drive Mach-Zehnder modulator-based single side-band modulation direct detection system without signal-to-signal beating interference," *J. Lightw. Technol.,* vol. 38, no. 16, pp. 4341–4351, Aug. 2020.

[9] X. Ruan, L. Zhang, F. Yang, Y. Zhu, Y. Li, and F. Zhang, "Beyond 100G single sideband PAM-4 transmission with silicon dual-drive MZM," *IEEE Photon. Technol. Lett.,* vol. 31, no. 7, pp. 509–512, Apr. 2019.

[10] X. Li et al., "Transmission of 4×28-Gb/s PAM-4 over 160-km single mode fiber using 10G-class DML and photodiode," in *Proc. Opt. Fiber Commun. Conf. Exhib.*, Anaheim, CA, USA, 2016, pp. 1–3.

[11] S. Searcy, G. Brochu, S. Boudreau, F. Trépanier, M. M. Filer, and S. Tibuleac, "Statistical evaluation of PAM4 data center interconnect system with slope-compensating fiber Bragg grating tunable dispersion compensation module," *IEEE J. Lightw. Technol.,* vol. 38, no. 12, pp. 3173–3179, Jun. 2020.

[12] R. Rath, D. Clausen, S. Ohlendorf, S. Pachnicke, and W. Rosenkranz, "Tomlinson–Harashima precoding for dispersion uncompensated PAM-4 transmission with direct-detection," *IEEE J. Lightw. Technol.,* vol. 35, no. 18, pp. 3909–3917, Sep. 2017.

[13] Z. Xing et al., "Experimental demonstration of 600 Gb/s net rate PAM4 transmissions over 2 km and 10 km with a 4-λ CWDM TOSA," *IEEE J. Lightw. Technol.,* vol. 38, no. 11, pp. 2968–2975, Jun. 2020.

[14] Y. Yu, M. R. Choi, T. Bo, Z. He, Y. Che, and H. Kim, "Low-complexity second-order Volterra equalizer for DML-based IM/DD transmission system," *IEEE J. Lightw. Technol.,* vol. 38, no. 7, pp. 1735–1746, Apr. 2020.

[15] H. Wang et al., "Adaptive channel-matched detection for C-Band 64-Gbit/s optical OOK system over 100-km dispersion-uncompensated link," *IEEE J. Lightw. Technol.,* vol. 38, no. 18, pp. 5048–5055, Sep. 2020.

[16] Z. Li et al., "Signal-signal beat interference cancellation in spectrally-efficient WDM direct-detection Nyquist-pulse-shaped 16-QAM subcarrier modulation," *Opt. Exp.,* vol. 23, no. 18, pp. 23694–23709, Aug. 2015.

[17] M. Xiang et al., "Advanced DSP enabled C-Band 112 Gbit/s/λ PAM-4 transmissions with severe bandwidth-constraint," *IEEE J. Lightw. Technol.,* vol. 40, no. 4, pp. 987–996, Feb. 2022.

[18] H. Wang et al., "Multi-rate Nyquist-SCM for C-band 100 Gbit/s signal over 50 km dispersion-uncompensated link," *J. Lightw. Technol.,* vol. 40, no. 7, pp. 1930–1936, Apr. 2022.

[19] L. Nadal et al., "DMT modulation with adaptive loading for high bit rate transmission over directly detected optical channels," *IEEE J. Lightw. Technol.,* vol. 32, no. 21, pp. 4143–4153, Nov. 2014.

[20] R. W. Gerchberg and W. O. Saxton, "A practical algorithm for the determination of the phase from image and diffraction plane pictures," *Optik,* vol. 35, no. 2, pp. 237–246, 1972.

[21] A. S. Karar, "Iterative algorithm for electronic dispersion compensation in IM/DD systems," *J. Lightw. Technol.,* vol. 38, no. 4, pp. 698–704, Feb. 2020.

[22] X. Wu, A. Karar, K. Zhong, A. Lau, and C. Lu, "Experimental demonstration of pre-electronic dispersion compensation in IM/DD systems using an iterative algorithm," *Opt. Exp.,* vol. 29, no. 16, pp. 24735–24749, Aug. 2021.

[23] G. Goeger, C. Prodaniuc, Y. Ye, and Q. Zhang, "Transmission of intensity modulation-direct detection signals far beyond the dispersion limit enabled by phase-retrieval," in *Proc. IEEE Eur. Conf. Opt. Commun.*, Valencia, Spain, 2015, pp. 1–3.

[24] H. Chen, N. K. Fontaine, J. M. Gene, R. Ryf, D. T. Neilson, and G. Raybon, "Dual polarization full-field signal waveform reconstruction using intensity only measurements for coherent communications," *J. Lightw. Technol.,* vol. 38, no. 9, pp. 2587–2597, May 2020.

[25] S. Hu, J. Zhang, J. Tang, W. Jin, R. Giddings, and K. Qiu, "Data-aided iterative algorithms for linearizing IM/DD optical transmission systems," *IEEE J. Lightw. Technol.,* vol. 39, no. 9, pp. 2864–2872, May 2021.

[26] S. Hu et al., "Multi-constraint Gerchberg-Saxton iteration algorithms for linearizing IM/DD transmission systems," *Opt. Exp.,* vol. 30, no. 6, pp. 10019–10031, Mar. 2022.